

EVALUATION OF A RESEARCH CIRCULATION  
CONTROL AIRFOIL USING NAVIER-STOKES METHODS

George D. Shrewsbury  
Advanced Flight Sciences Department  
Lockheed-Georgia Company, Marietta, Georgia

Abstract

The compressible Reynolds time averaged Navier-Stokes equations were used to obtain solutions for flows about a two-dimensional circulation control airfoil. The governing equations were written in conservation form for a body-fitted coordinate system and solved using an Alternating Direction Implicit (ADI) procedure. A modified algebraic eddy viscosity model was used to define the turbulent characteristics of the flow, including the wall jet flow over the Coanda surface at the trailing edge. Numerical results are compared to experimental data obtained for a research circulation control airfoil geometry. Excellent agreement with the experimental results was obtained.

Introduction

One of the most efficient of the various methods for generating increased lift is the circulation control (CC) airfoil. This concept was developed in England<sup>1-2</sup> and introduced into the United States by U.S. Navy researchers<sup>3-5</sup>. It has subsequently been the subject of extensive experimental test programs which have confirmed the high-lift capability of this innovative concept<sup>6-9</sup>. These airfoils obtain lift augmentation by tangentially exhausting a thin jet sheet over a rounded trailing edge with the jet sheet remaining attached well onto the airfoil lower surface due to the Coanda effect.

Formerly, analysis methods for CC airfoils<sup>10-13</sup> consisted of computational procedures which used weakly coupled viscous-inviscid procedures to define the complex flow fields resulting from the presence of the jet sheet exhausting into the trailing edge region. Particularly good results were obtained by using a potential flow CC airfoil solver developed by Dvorak, et al<sup>11,13</sup> coupled with a parabolized Navier-Stokes wall-jet analysis program written by Dash, and associates<sup>12</sup>.

The complex flow fields of the CC airfoil are governed by highly interactive flow regimes, however, and a comprehensive analysis of the flow field and the associated phenomena, including the effects of jet entrainment and Coanda surface geometry, requires analysis procedures which account for the strongly coupled nature of the viscous and inviscid flow regimes.

Recently, Navier-Stokes methods have been used successfully to solve for the aerodynamics about CC airfoils<sup>14-17</sup>. The purpose of this paper is to present the results obtained by using the method developed in reference 15



to correlate numerical results with performance data from an extensive experimental study<sup>18</sup>. This method solves the fully elliptic Navier-Stokes equations in 2-D planar coordinates. The mathematical and numerical formulations are discussed, and appropriate boundary conditions and grid generation procedures are defined. Modifications to existing eddy viscosity turbulence models to account for curved wall jets are discussed.

## Method

### Mathematical Formulation

The development of the two-dimensional, unsteady, compressible Navier-Stokes equations used for this study are documented in Reference 19, and refinements to the method are reported in References 20-22.

The compressible Reynolds time averaged Navier-Stokes equations may be written in vector form as follows:

$$\frac{\partial}{\partial \tau}[\hat{q}] + \frac{\partial}{\partial \xi}[\hat{F}] + \frac{\partial}{\partial \eta}[\hat{G}] = \frac{1}{Re} \left\{ \frac{\partial}{\partial \xi}[\hat{F}_1] + \frac{\partial}{\partial \eta}[\hat{G}_1] \right\} \quad (1)$$

Here  $\xi$ ,  $\eta$ , and  $\tau$  are the independent variables subject to the general transformation:

$$\begin{aligned} \xi &= \xi(x, y, t) \\ \eta &= \eta(x, y, t) \\ \tau &= t \end{aligned} \quad (2)$$

and:

$$\begin{aligned} [\hat{q}] &= \frac{1}{J} [\vec{q}] \\ [\hat{F}] &= \frac{1}{J} [\epsilon_t \vec{q} + \epsilon_x \vec{F} + \epsilon_y \vec{G}] \\ [\hat{G}] &= \frac{1}{J} [\eta_t \vec{q} + \eta_x \vec{F} + \eta_y \vec{G}] \\ [\hat{F}_1] &= \frac{1}{J} [\epsilon_x \vec{F}_1 + \epsilon_y \vec{G}_1] \\ [\hat{G}_1] &= \frac{1}{J} [\eta_x \vec{F}_1 + \eta_y \vec{G}_1] \end{aligned} \quad (3)$$

where:

$$\begin{aligned}
 \vec{q} &= \begin{pmatrix} \rho \\ \rho u \\ \rho v \\ \rho E \end{pmatrix} & \vec{F} &= \begin{pmatrix} \rho u \\ \rho u^2 + p \\ \rho uv \\ (\rho E + p)u \end{pmatrix} \\
 \vec{G} &= \begin{pmatrix} \rho \\ \rho uv \\ \rho v^2 + p \\ (\rho E + p)v \end{pmatrix} & \vec{F}_1 &= \begin{pmatrix} 0 \\ \tau_{xx} \\ \tau_{xy} \\ \frac{\gamma}{Pr} k \frac{\partial e}{\partial x} + u\tau_{xx} + v\tau_{xy} \end{pmatrix} & \vec{G}_1 &= \begin{pmatrix} 0 \\ \tau_{xy} \\ \tau_{yy} \\ \frac{\gamma}{Pr} k \frac{\partial e}{\partial y} + u\tau_{xy} + v\tau_{yy} \end{pmatrix}
 \end{aligned} \tag{4}$$

The components of the viscous stress tensor are given by

$$\begin{aligned}
 \tau_{xx} &= (\lambda + 2\mu) \frac{\partial u}{\partial x} + \lambda \left( \frac{\partial v}{\partial y} \right) \\
 \tau_{yy} &= (\lambda + 2\mu) \frac{\partial v}{\partial y} + \lambda \left( \frac{\partial u}{\partial x} \right) \\
 \tau_{xy} &= \mu \left( \frac{\partial u}{\partial y} + \frac{\partial v}{\partial x} \right)
 \end{aligned} \tag{5}$$

where  $p$  is the pressure,  $\rho$  is the density,  $\mu$  is the bulk viscosity,  $e$  is the specific internal energy, and  $\lambda$  is taken as  $-2/3 \mu$ , according to Stoke's hypothesis. The viscosity,  $\mu$ , is defined by Sutherland's law. The equation of state:

$$p = \rho RT$$

is required for closure of the system of equations.

In the above equations, all distances are normalized with respect to the airfoil chord, the velocities are normalized with respect to the free stream velocity,  $V_\infty$ , the density is normalized with respect to the free stream density, and the specific internal energy is normalized with respect to  $V_\infty^2$ .  $Re$  and  $Pr$  are the Reynolds number and Prandtl number, respectively.

#### Numerical Formulation

The numerical procedure used to solve the system of governing equations is a modified form of the Briley-McDonald<sup>23</sup> Alternating Direction Implicit (ADI) procedure, which is based on the Douglas-Gunn<sup>24</sup> method. It is also closely related to the Warming-Beam<sup>25</sup> algorithm. Variable time steps and numerical dissipation have been incorporated to accelerate the convergence for steady state flow problems.

The method can be outlined as follows: The governing equations are parabolic with respect to time. Assuming the flow field is known at a time level  $t_n$ , the numerical procedure is used to advance the solution to a new time level  $t_{n+1}$  using a fairly large time step. If a steady state solution is desired, the procedure at each cell is advanced at a different time step based on the local cell Reynolds number. The metric terms  $\xi_x$ ,  $\xi_y$ , etc., are evaluated numerically at an intermediate time level  $t_{n+1/2}$ . The mixed

derivatives that arise from terms such as  $(\xi_x U \tau_{xx})$ , etc., are lagged one time step. The flow quantities  $\rho$ ,  $u$ ,  $v$ , and  $e$  at the new time level are written in terms of their values at the known time level and the incremental quantities; i.e.,

$$\rho^{n+1} = \rho^n + \Delta\rho^n$$

The non-linear terms involved are linearized by using a Taylor expansion about the solution at the known time level  $t_n$ . Performing these operations and taking all the known quantities to the right hand side, one obtains a linear system of equations for the incremental quantities at each grid point in the computational plane, excluding the boundaries. The difference equations may be written in matrix form as:

$$[A] (\Delta q)^n + \frac{\partial}{\partial \xi} [b] (\Delta q)^n + \frac{\partial}{\partial \eta} [c] (\Delta q)^n = [R]^n \quad (6)$$

The Douglas-Gunn procedure for generating an ADI scheme is used to solve the above system of equations by approximate factorization of equation (6) into two equations, where each involves only a one-dimensional operator:

$$[A] (\Delta q)^* + \frac{\partial}{\partial \xi} [B] (\Delta q)^* = [R]^n \quad (7)$$

$$[A] (\Delta q)^n + \frac{\partial}{\partial \eta} [C] (\Delta q)^n = [A] (\Delta q)^* \quad (8)$$

where

$$\{\Delta q\} = \{\Delta\rho, \Delta u, \Delta v, \Delta e\}^T \quad (9)$$

Equations (7) and (8) are discretized using second order accurate difference formulas for the spatial derivatives. This technique results in a matrix system with a block tridiagonal structure which may be solved efficiently by using standard block elimination procedures. The boundary conditions for the unknown vector  $\{\Delta g\}$  are evaluated explicitly. Once  $\{\Delta g\}^n$  is obtained, the flow field variables at the new time level are explicitly known.

#### Artificial Dissipation Terms

To suppress the high frequency components that appear in regions containing severe pressure gradients, i.e., the neighborhood of shock waves or stagnation points, artificial dissipation terms have been added in conservative form. In the present application, a blend of second and fourth order terms with coefficients which depend on the magnitude of the local pressure gradient have been added explicitly for each dependent variable in the manner suggested by Jameson<sup>26</sup>, et al., and second order dissipation

terms have been added implicitly for each of the dependent variables. The coefficients of the implicit terms were added in the manner suggested by Steger<sup>27</sup>. Extensive numerical experiments have shown that the blending of the dissipation terms provided better shock wave prediction with controlled overshoot pressure distribution.

### Turbulence Model

An algebraic eddy viscosity model developed by Baldwin and Lomax<sup>28</sup> was used to define the turbulence transport everywhere except in the wall jet free shear layer. This model permits the calculation of the turbulence characteristics of the boundary layer by defining a two layer system. The viscosity in the inner layer is given by simple mixing length theory, where the length scale is proportional to the distance from the wall multiplied by the van Driest damping term, and the velocity scale is proportional to the length multiplied by the absolute value of the vorticity

$$\nu_{t\text{INNER}} = \rho l^2 |\omega| \quad (10)$$

where

$$l = ky [1 - \exp(-y^+/\Lambda^+)] \quad (11)$$

In the outer layer, the velocity and length scales are constant and the turbulent viscosity is calculated from:

$$\nu_{t\text{OUTER}} = K C_{cp} \rho F_{\text{WAKE}} F_{\text{KLEB}} \quad (12)$$

$F_{\text{WAKE}}$  is defined as the minimum value of

$$y_{\text{MAX}} F_{\text{MAX}}$$

or

$$C_{WK} y_{\text{MAX}} U_{\text{DIFF}}^2 / F_{\text{MAX}}$$

$F_{\text{MAX}}$  is determined from the maximum value of

$$F(y) = y |\omega| [1 - \exp(-y^+/\Lambda^+)] \quad (13)$$

and  $y_{\text{MAX}}$  is defined as the  $y$  at which  $F_{\text{MAX}}$  occurs.  $F_{\text{KLEB}}$  and  $U_{\text{DIFF}}$  are defined by

$$F_{\text{KLEB}} = \left\{ 1 + 5.5 \left( \frac{C_{\text{KLEB}} y}{y_{\text{MAX}}} \right)^6 \right\}^{-1}$$

$$U_{\text{DIFF}} = \left( \sqrt{U^2 + v^2} \right)_{\text{MAX}} - \left( \sqrt{U^2 + v^2} \right)_{\text{MIN}}$$

The constants used in these equations are defined in Reference 28.

The division between the inner and outer layers is taken as that point at which

$$\nu_{t\text{OUTER}} = \nu_{t\text{INNER}}$$

The turbulence characteristics of the curved wall jet on the Coanda surface require special treatment, since the extra rates of strain produced by the curvature can exert an influence on the turbulence structure by augmenting or suppressing radial velocity fluctuations. In a curved wall jet, such as that shown in Figure 1, a balance of centrifugal and pressure forces on a fluid element reveals that increases in velocity with distance from the center of streamline curvature generate stable flows, while flows in which the velocity decreases from the center of curvature are destabilized<sup>29</sup>. In turbulent flow, these stabilities and instabilities lead to an increase or decrease in turbulent transport. This influence can result in viscosities which are an order of magnitude greater than those obtained in planar flows<sup>30</sup>. Accordingly, turbulence models using standard eddy viscosity relations will require significant empirical modifications to reproduce the characteristics of curved shear layer flows. For this study, the mixing length was multiplied by an empirical curvature correction

$$F = 1 - \alpha S$$

where  $\alpha$  is an empirical constant whose value depends on the particular flow considered. A review of the literature suggests that most researchers place the constant in the range  $6 < \alpha < 14$  for wall bounded flows. For this study, however, a value of 25 produced results more nearly in agreement with experimental data.  $S$  is a dimensionless parameter which is representative of the ratio of the extra rate of strain produced by the curvature to the inherent shear strain

$$S = \frac{U/r}{\partial U / \partial n}$$

where  $U$  is the velocity in the streamwise direction,  $n$  is the normal direction, and  $r$  is the local radius of curvature of the streamline considered. In areas where the curvature is small to moderate, the correction to the eddy viscosity is negligible.

The location of the wake was approximated by determining the point, nearest the trailing edge, at which the  $U$  component of the contravariant velocity at the second grid line changed direction. The wake was then arbitrarily defined to exist in the region contained in the four grid points on each side of that location. The calculation of the eddy viscosity began at the lower edge of the wake, and proceeded clockwise to the upper edge of the wake. Values of the turbulent viscosity for the wake were then interpolated linearly from the values at the wake edges.

#### Grid Generation and Boundary Conditions

A body-fitted coordinate system is desired for numerical analysis procedures since boundary surfaces in the physical plane are mapped onto rectangular surfaces in the transformed plane, and the boundary conditions in the transformed plane may be treated more accurately. Computer methods developed by Thomas<sup>31</sup> were employed to generate a suitable body-fitted, curvilinear grid system. This procedure uses a Poisson solver to define two-dimensional grids about airfoils and other shapes.

The unique trailing edge geometry and flow characteristics of CC airfoils makes the use of conventional C-grids difficult, since it is impossible to locate the cut line so that it corresponds to the physical location of the wake. Consequently, it was decided to use an O-grid topology for this analysis. This choice represents a compromise between suitable resolution on the Coanda surface and adequate definition in the near-wake region.

The grid spacing in the direction normal to the airfoil surface was sufficiently dense to permit satisfactory resolution of the boundary layer. Sixty-one grid lines were used in this direction, and approximately twenty of these were submerged in the boundary layer. The grid spacing in the normal direction varied from 0.00007 chords at the wall to 0.60 chords at the outer boundary. The outer boundary was defined as circular, and was fourteen chords in diameter. One-hundred and fifty-one points were used in the wrap-around direction. Grid points were clustered to permit satisfactory resolution at critical locations, such as the leading edge and blowing slot exit planes. One of the computational grids used for this study is shown in Figure 2.

Boundary conditions for the computational plane consisted of specifying the flow conditions along the airfoil surface, including the blowing slot exit plane, the O-grid cut line, and the outer boundary. On the airfoil surface, an adiabatic wall condition,  $\partial e / \partial \eta = 0$ , was imposed and extrapolated values of density were specified. A no-slip condition ( $u = v = 0$ ) was used to define the velocities. At the slot blowing exit, specified values of total pressure and total temperature were used with an extrapolated value of pressure to define the boundary characteristics. Along the grid cut line, boundary conditions were applied explicitly as the average of the extrapolated values from each direction.

At the outer boundary, conditions were applied according to the rule that flow variables should be extrapolated along characteristics leaving the cell and specified along characteristics entering the cell. Accordingly, for subsonic conditions where the boundary is experiencing inflow, values of the velocity and pressure are specified, while the energy is extrapolated from the interior. For outflow conditions, the pressure is specified, while values of velocity and energy are extrapolated from the interior. Numerical disturbances generated by the body may be reflected back into the computational plane, creating an adverse influence on the convergence characteristics of the solution. To eliminate the reflection of unwanted propagations, the pressure is specified according to non-reflecting boundary criteria prescribed by Rudy and Strikwerda<sup>32</sup>, which have been implemented at the outflow boundaries.

In all cases where extrapolated values were specified at the boundaries, a two-point extrapolation of the form

$$q_1 = \frac{4}{3} q_2 - \frac{1}{3} q_3$$

was used.

## Results

## Research CC Airfoil

Novak and Cornelius<sup>18</sup> conducted wind tunnel tests on a 15.6 per cent thick CC airfoil section which had been specifically designed to provide data for Navier-Stokes code validation. The blowing slot height-to-radius ratio was 0.1, and the overall chord length was 15 inches. This model was designed with a cylindrical Coanda surface with a radius-to-chord ratio of 0.067. While this ratio is relatively high and is certainly not representative of practical flight systems, it does provide a physically large slot height, which improves the quality of the measurements. Data were acquired in the Lockheed-Georgia Low Turbulence Wind Tunnel at a free-stream Mach number of 0.0853 and a Reynolds number of 780,000. The model angle of attack was zero degrees. The data consisted of airfoil surface pressure measurements and extensive flow field surveys using a laser velocimeter (LV). The general profile of the section can be visualized from the grid shown in Figure 2.

Once a suitable computational grid had been constructed, numerical studies were conducted at a Mach number and Reynolds number corresponding to the experimental tests. The angle of attack was varied numerically until a lift coefficient based on integrated pressures was obtained which corresponded to the experimental zero incidence case. For the jet total pressure ratio investigated, the numerical angle of attack was -2 degrees, and the corresponding lift coefficient was 4.55. All computed and experimental data subsequently presented are for that lift coefficient. The jet total pressure ratio was 1.10, and the ratio of jet total temperature to free-stream total temperature was .964.

The numerical results were obtained by executing the code on the Lockheed/ASG Cray X-MP/24 computer. Approximately 1000 iterations were required to obtain a converged, steady-state solution. This formulation of the Navier-Stokes equations requires approximately  $2.5 \times 10^{-4}$  CPU seconds/grid-point/time-step of Cray execution time.

Computed streamlines for the research airfoil are shown in Figure 3. This figure clearly demonstrates the characteristic flows for CC airfoils, including the large, induced circulation which produces a strong downwash in the wake region and upwash at the leading edge. The jet entrainment effects on the upper surface and the Coanda turning of the jet can also be seen.

Computed velocity vectors and streamlines in the trailing edge region are shown for the same case in Figure 4. Details of wall jet development, as well as the interaction of the upper and lower surface flows can be clearly visualized. These results demonstrate the attached, well-behaved nature of the flow, which is characteristic of CC airfoils, even near stall<sup>6</sup>.

Comparisons of computed and experimental velocity profiles at the jet exit plane are shown in Figure 5. The profiles are shown as ratios of the local velocity to the free-stream velocity versus the radial distance above the Coanda surface. The upper edge of the exhaust jet is located at a Y of .1 inches. The data in Figure 5(a) include the boundary layer which has been established on the airfoil upper surface as well as the jet slot exhaust flow. The comparison between the computed and experimental boundary layers

is very good, which suggests that the jet entrainment effects propagated upstream are being properly modeled.

A detailed comparison of the computed and experimental velocity profiles for the jet exhaust is shown in Figure 5(b). In order to produce corresponding values of jet exhaust velocities, the numerical data were run at a jet total pressure ratio of 1.10, compared to a value of 1.12 measured experimentally. The discrepancy may be due to total pressure losses experienced in the duct between the plenum measurement location and the jet exit plane. The numerical total pressure ratio used however, provides an excellent reproduction of the experimental velocity profile except at the upper edge of the jet, where an established jet boundary layer already existed. The consequences of failing to properly model this characteristic of the jet exhaust profile are not known.

The jet exit total pressure was assumed to be constant across the jet slot height except at the walls, where a no-slip ( $u = v = 0$ ) condition was enforced. The small velocity deficit occurring near the bottom of the numerical profile is believed to be the result of errors introduced by poor grid characteristics in that region. The comparison between the computed and experimental velocity gradients produced by the strong radial pressure differentials is very good. The numerical velocities obtained from this total pressure ratio resulted in a jet momentum coefficient of approximately 0.275.

It is interesting to note that the differences in experimental boundary layers observed at the upper and lower edges of the jet are consistent with the previously discussed postulate that positive radial velocity gradients in regions of curvature are stabilizing, while negative velocity gradients in that direction are destabilizing.

Experimental and computed velocity profiles for the wall jet flow at a circumferential location of 90 degrees, measured clockwise from the jet exit location, are shown in Figure 6. The conditions at which these results were obtained are the same as for the previous figure. While the general magnitudes and wall jet thicknesses agree reasonably well, the differences in profile characteristics near the wall are significant. The extremely stable characteristics exhibited by the experimental flow adjacent to the wall are not reproduced adequately by the numerical data. Since the experimental conditions at the beginning of the Coanda region are closely approximated, it is concluded that an empirically corrected eddy viscosity turbulence formulation is not sufficient to properly model the turbulent characteristics of curved wall jets, particularly the strong stabilization that occurs near the boundary. As a consequence of this discrepancy, the numerical wall jet dissipates energy too rapidly and experiences premature detachment. The angle of attack correction of -2 degrees was underpredicted therefore, and the actual equivalent experimental angle of attack was somewhat more negative.

Experimental and computed CC airfoil pressure distributions are shown in Figure 7. The agreement between experimental and computed pressure distributions is very good. The strong suction peaks produced by the super-circulation at the leading edge and the jet sheet turning on the Coanda surface are very accurately predicted. The discrepancy between the computed and experimental data on the lower surface, near the trailing

edge, is probably the result of differences in the locations of the jet sheet detachment points, as observed experimentally and predicted numerically.

### Conclusions

A computational procedure has been developed which permits the calculation of the performance characteristics of circulation control airfoils over a broad range of free-stream conditions. The fully elliptic, Reynolds time averaged Navier-Stokes equations were solved numerically, using an Alternating Direction Implicit (ADI) algorithm. The computed results compared well with experiments conducted on a research CC airfoil which had been specifically designed to provide data for Navier-Stokes code validation, including force data and detailed flow measurements taken in the trailing edge region. A specially modified algebraic eddy viscosity model was used to predict the behavior of the wall jet, and although the overall behavior of the curved wall jet was sufficiently approximated, important turbulent characteristics crucial to the prediction of the jet sheet detachment point were not adequately predicted. Extensions to the present work will include the incorporation of advanced turbulence models to provide improved analysis of the wall jet characteristics.

### References

1. Cheeseman, I.C., and Seed, A.R., "The Application of Circulation Control by Blowing to Helicopter Rotors," lecture to the Royal Aeronautical Society (Feb. 1966), published in J.R.Ae.S., vol 71, no. 848, July 1966.
2. Kind, R.J., "A Calculation Method for Circulation Control by Tangential Blowing Around a Bluff Trailing Edge," Aeronautical Quarterly, Vol. XIX, August 1968, pp 205-233.
3. Williams, R.M., "Some Research on Rotor Circulation Control," Proc. of the Third Cal/AVLABS Symp., Vol. 11, June 1969.
4. Williams, R.M. and Howe, H.J., "Two-Dimensional Subsonic Wind Tunnel Tests On a 20% Thick, 5% Cambered Circulation Control Airfoil," NSRDC TN AL-176, August 1970.
5. Englar, Robert J., "Two-Dimensional Transonic Wind Tunnel Tests of Three 15-percent Thick-Circulation Control Airfoils," NSRDC Report ASED-182, December 1970.
6. Abramson, J. and Rogers, E.O., "High-Speed Characteristics of Circulation Control Airfoils," AIAA Paper 83-0265, Jan. 1983.
7. Loth, J.L. and Boasson, M., "Circulation Controlled STOL Wing Optimization," AIAA Paper 83-0082, Jan. 1983.
8. Wood, N.J., "The Performance of a Circulation Control Airfoil at Transonic Speeds," AIAA Paper 83-0083, Jan. 1983.
9. Englar, R.J. and Huson, G.G., "Development of Advanced Circulation Control Wing High Lift Airfoils," AIAA Paper 83-1847, July 1983.

10. Gibbs, E.H. and Ness, N., "Analysis of Circulation Controlled Airfoils," TR-43, Department of Aerospace Engineering, West Virginia University, June 1975.
11. Dvorak, F.A. and Kind, R.J., "Analysis Method for Viscous Flow Over Circulation-Controlled Airfoils," Journal of Aircraft, Vol. 16, No. 1, January 1979.
12. Dash, S.M. and Wolf, D.E., "Viscous/Inviscid Analysis of Curved Wall Jets: Part 1 - Inviscid Shock Capturing Model (SCIPWJET)," SAI/PR TR-5, September 1982.
13. Dvorak, F.A. and Choi, D.H., "Analysis of Circulation-Controlled Airfoils in Transonic Flow," Journal of Aircraft, Vol. 20, No.4, April 1983.
14. Shrewsbury, George, "Numerical Evaluation of Circulation Control Airfoil Performance Using Navier-Stokes Methods," AIAA Paper 86-0286, January 1986.
15. Shrewsbury, George D., "Analysis of Circulation Control Airfoils Using an Implicit Navier-Stokes Solver," AIAA Paper 85-0171, January 1985.
16. Berman, H.A., "A Navier-Stokes Investigation of a Circulation Control Airfoil," AIAA Paper 85-0300, January 1985.
17. Pulliam, Thomas H., Jespersen, Dennis C., and Barth, Timothy J., "Navier-Stokes Computations for Circulation Controlled Airfoils," AIAA Paper 85-1587, July, 1985.
18. Novak, Charles J. and Cornelius, Kenneth C., "An LDV Investigation of a Circulation Airfoil Flowfield," AIAA Paper 86-0503, January, 1986.
19. Tassa, Y., "An Implicit Method for Solving the Navier-Stokes Equations with Application to Shock Boundary Layer Interaction," Lockheed-Georgia Report LG79RR001, 1979.
20. Sankar, N.L. and Tassa, Y., "Reynolds Number and Compressibility Effects on Dynamic Stall of a NACA 0012 Airfoil," AIAA Paper 80-0010, Pasadena, CA., January 1980.
21. Shrewsbury, G.D. and Tassa, Y., "Numerical Simulation of Transonic Flow About Isolated Afterbodies," AIAA Paper 83-0498, January 1983.
22. Schuster, D.M. and Birckelbaw, L.D., "Numerical Computation of Viscous Flowfields about Multiple Component Airfoils," AIAA Paper 85-0167, Jan. 1985.
23. Briley, W.R., and McDonald, H., "An Implicit Numerical Method for Multidimensional Compressible Navier-Stokes Equations," Report M9113363-6, United Aircraft Research Laboratories, November 1973.
24. Douglas, J. and Gunn, J.E., "A General Formulation of Alternating Direction Methods," Numerische Math., Vol. 6, 1967, pp 428.

25. Beam, R., and Warming, R.F., "An Implicit Factored Scheme for Compressible Navier-Stokes Equations," AIAA Paper 77-645, June 1977.
26. Jameson, A., Schmidt, W., and Turkel, E., "Numerical Solutions of the Euler Equations by Finite Volume Methods Using Runge-Kutta Time-Stepping Schemes," AIAA 81-1259, Palo Alto, CA, 1981.
27. Steger, J.L., "Implicit Finite Difference Simulation of Flow About Arbitrary Two-Dimensional Geometries," AIAA Journal, Vol. 16, No. 4, July 1978, pp. 679-686.
28. Baldwin, B.S., and Lomax, H., "Thin Layer Approximation and Algebraic Model for Separated Turbulent Flows," AIAA Paper 78-257, Jan. 1978.
29. Wilson, D.J., and Goldstein, R.J., "Turbulent Wall Jets with Cylindrical Streamwise Surface Curvature," Journal of Fluids Engineering, September 1976, pp 550-557.
30. Rodi, W., and Scheurer, G., "Calculation of Curved Shear Layers with Two-Equation Turbulence Models," Phys. Fluids 26(6), June 1983, pp1422-1436.
31. Thomas, P.D., "Construction of Composite Three-Dimensional Grids From Subregion Grids Generated by Elliptic Systems," AIAA Journal, Vol. 20, No. 9, Sept. 1982, pp.1195,1202.
32. Rudy, D., and Strikwerda, J., "A Non Reflecting Outflow Boundary Condition for Subsonic Navier-Stokes Calculations," Journal of Computational Physics, Volume 36, pp. 55-70, 1980.

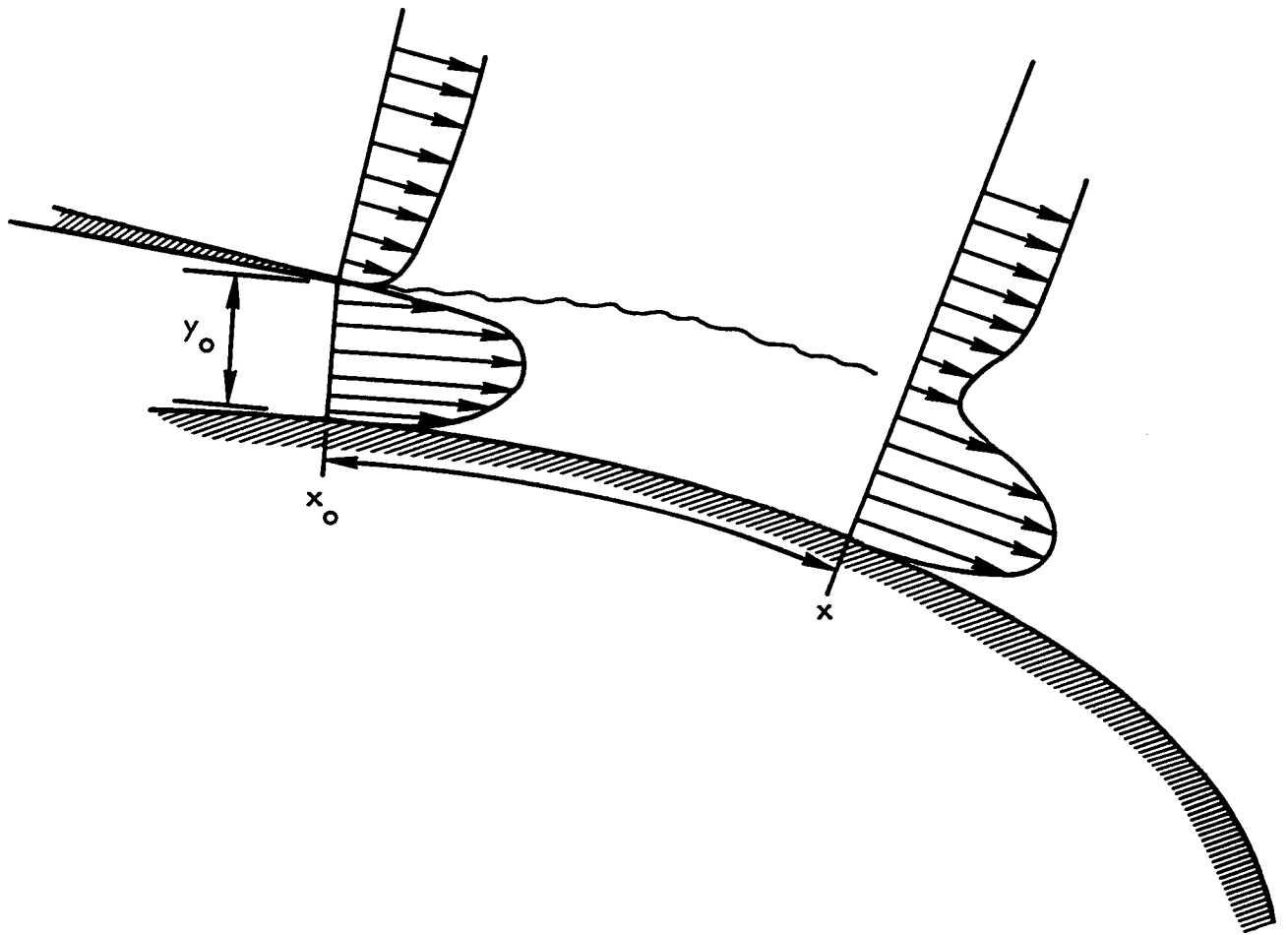


Figure 1. Wall-Jet/Coanda-Surface Nomenclature

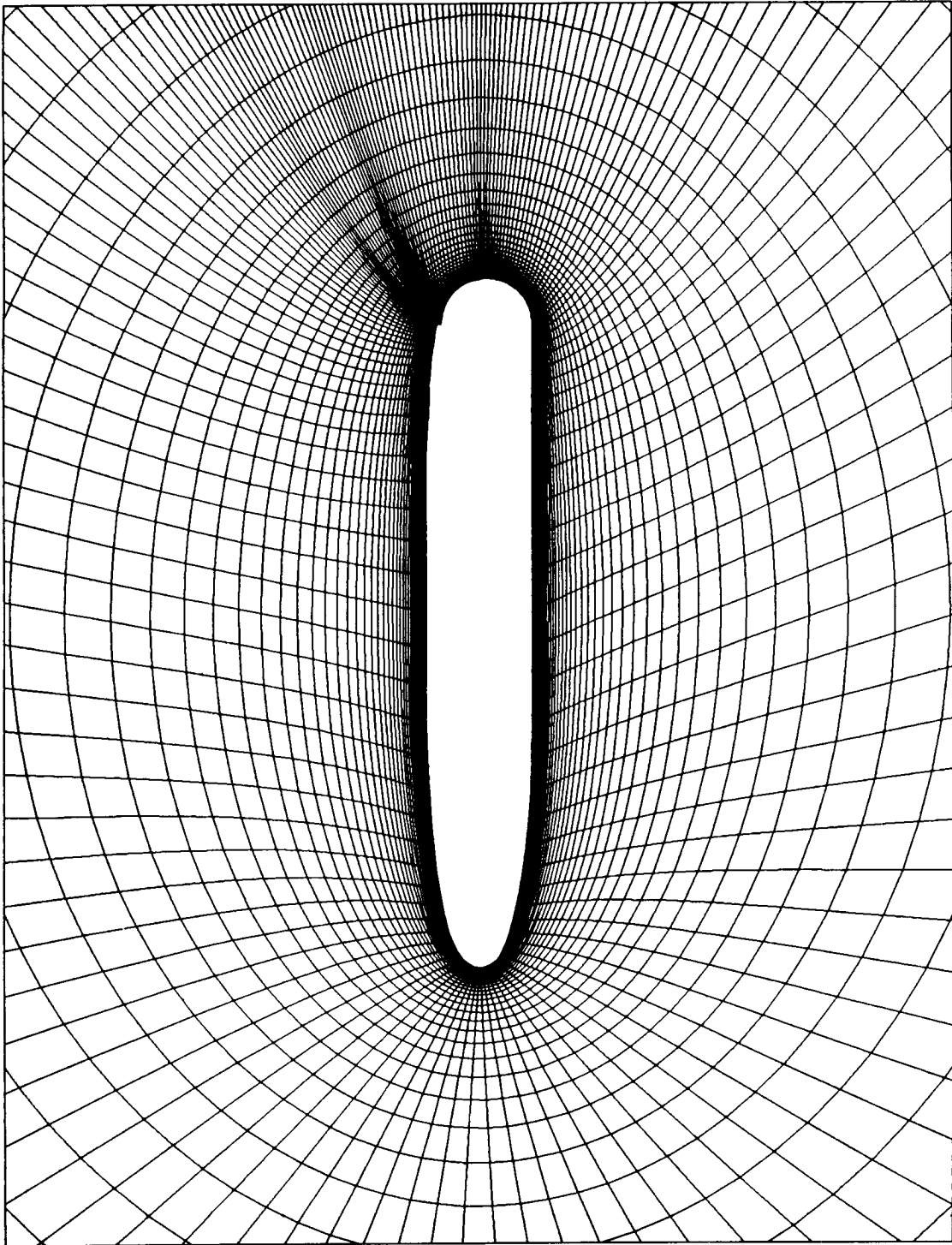


Figure 2. Computational Grid

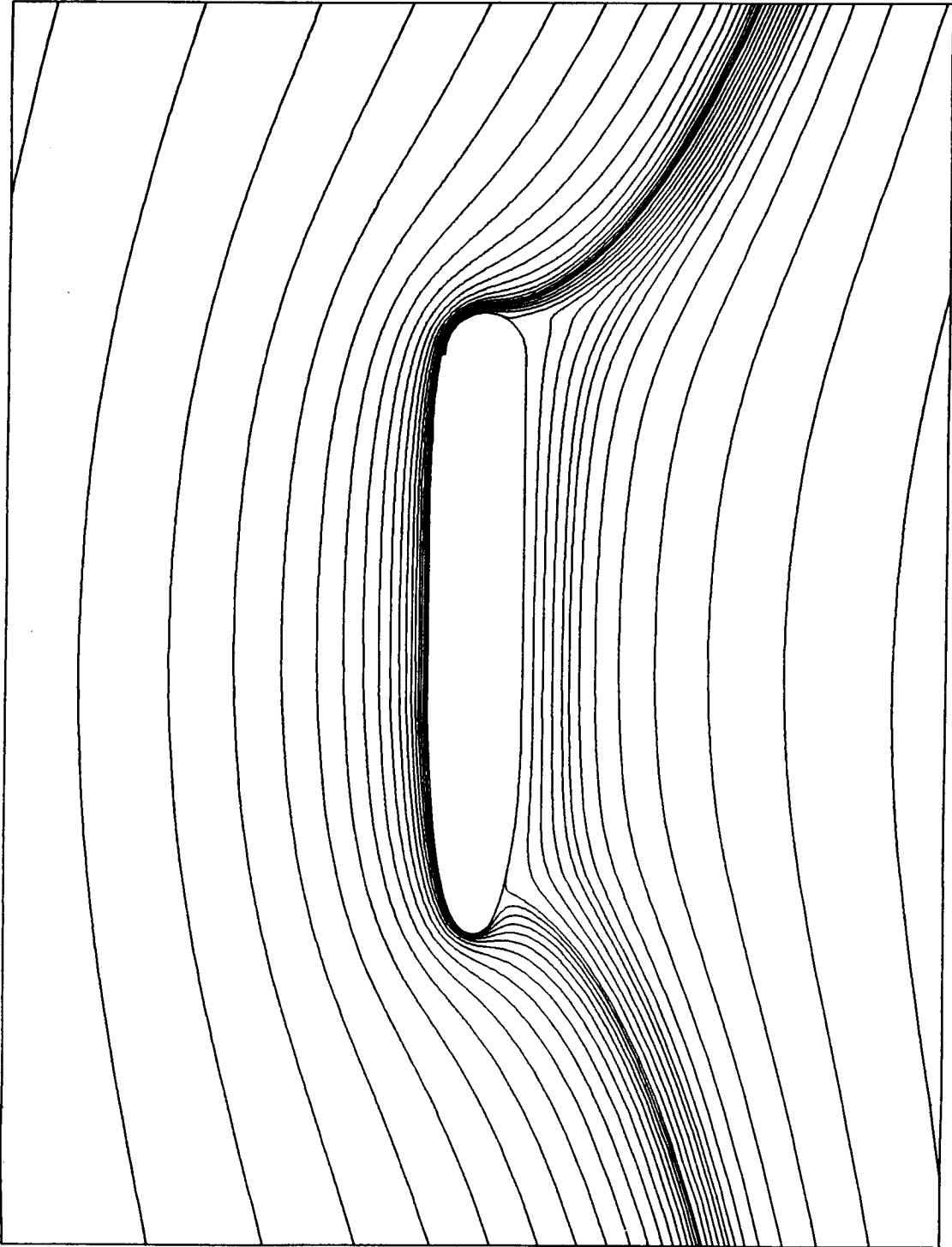


Figure 3. Computed Streamlines for Research CC Airfoil

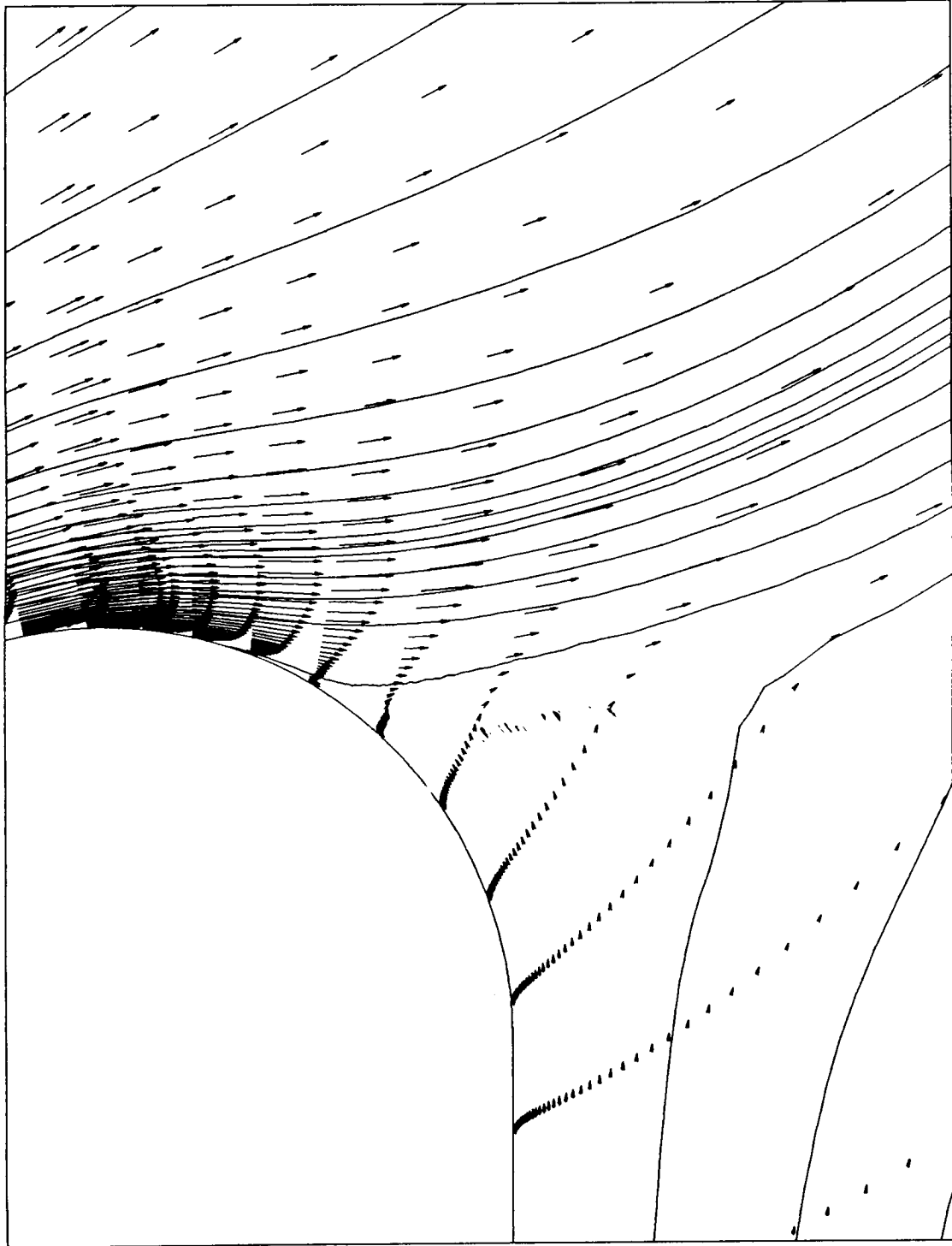


Figure 4. Computed Velocity Vectors and Streamlines

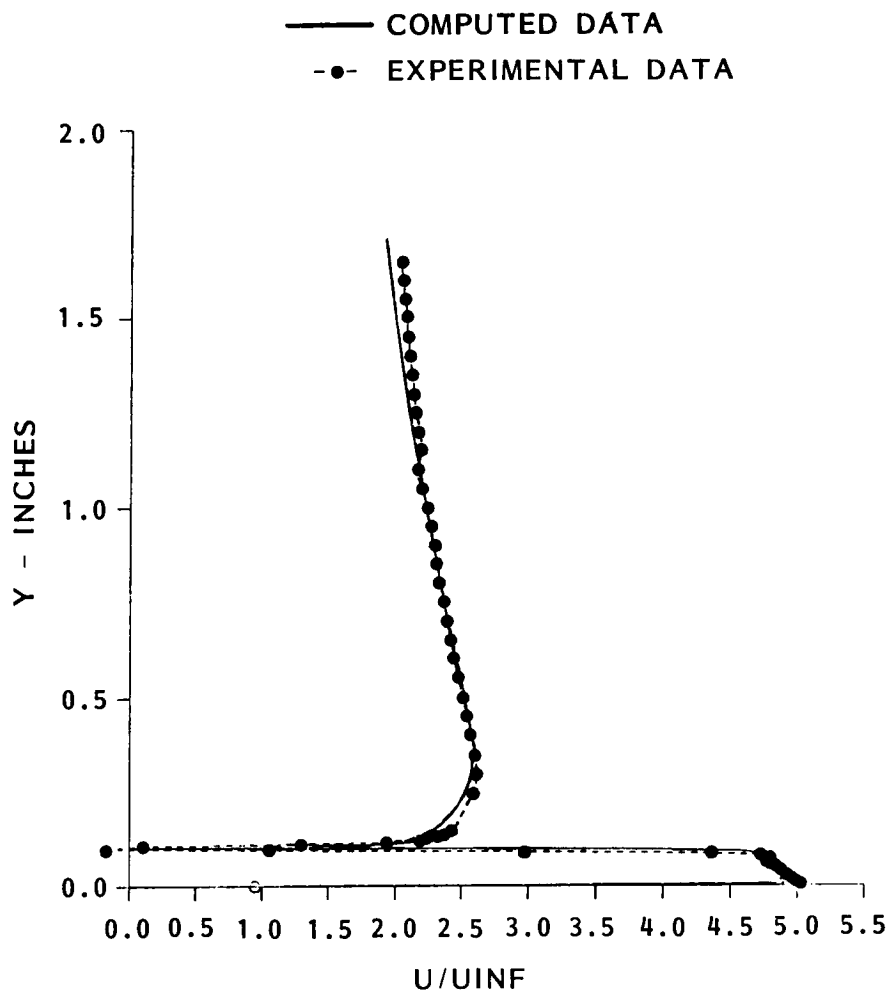


Figure 5(a). Computed and Experimental Velocity Profiles at Jet Exit Plane

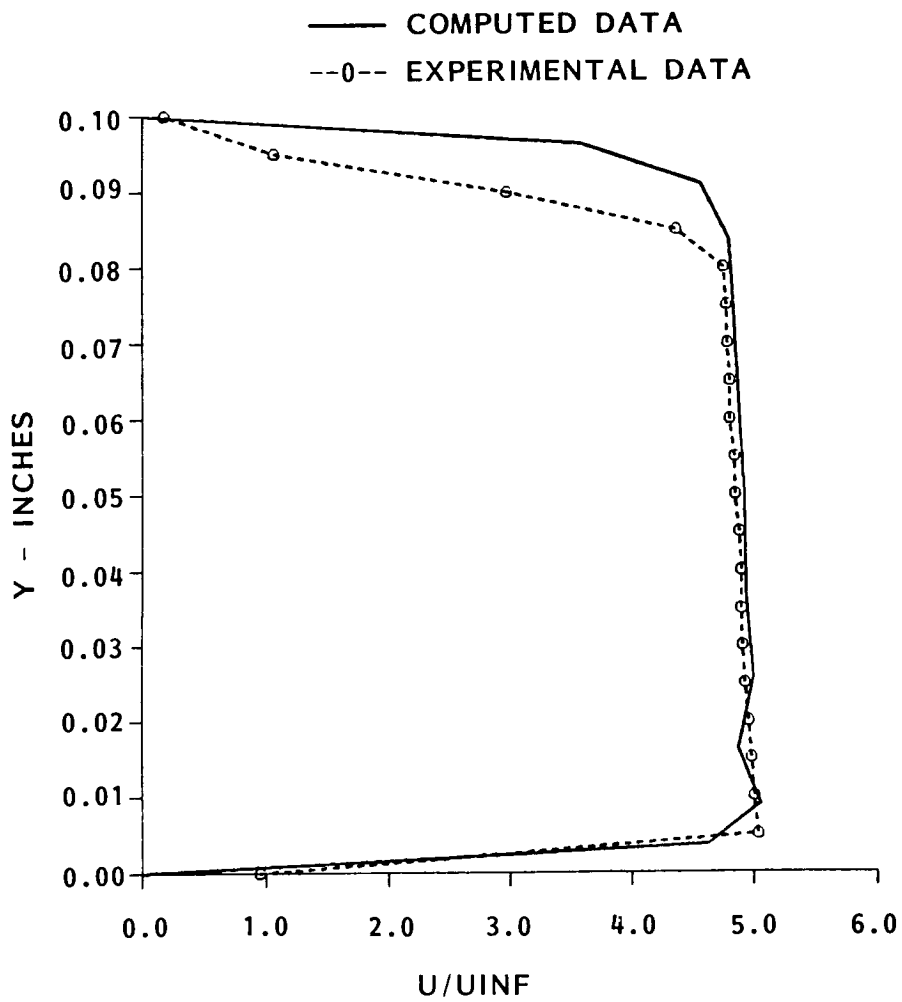


Figure 5(b). Computed and Experimental Velocity Profiles for Jet Slot Exit

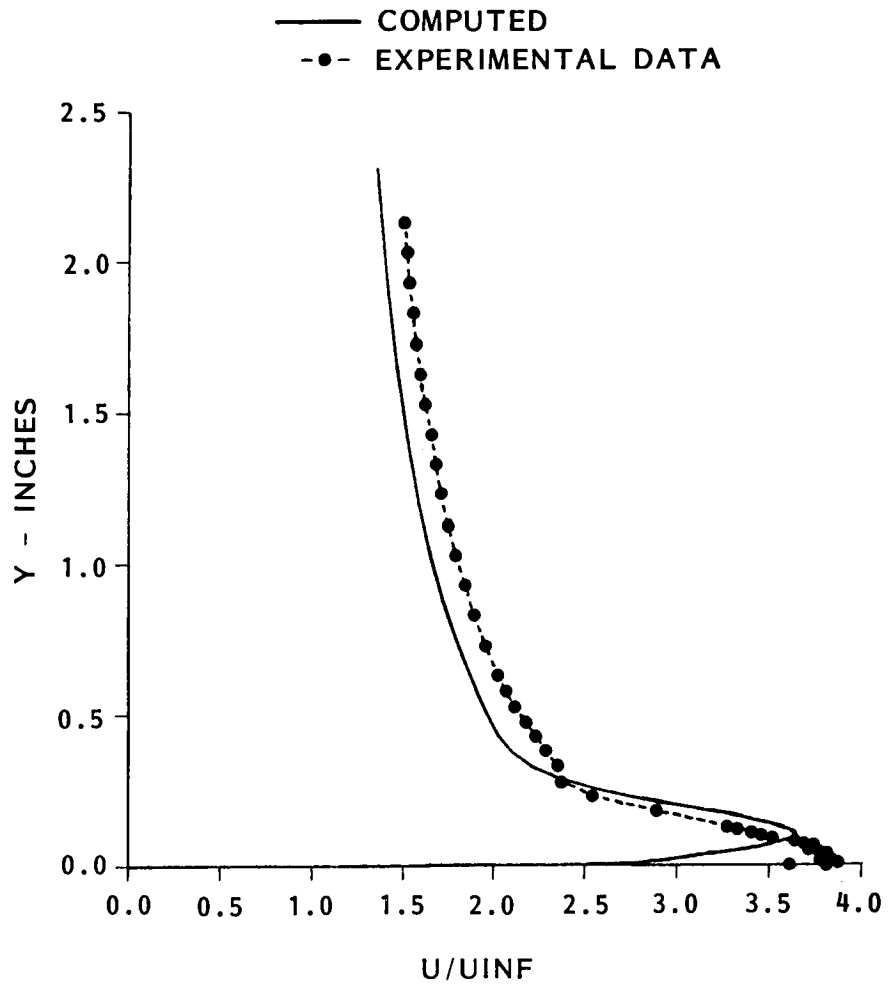


Figure 6. Computed and Experimental Velocity Profiles at Theta = 90 Degrees

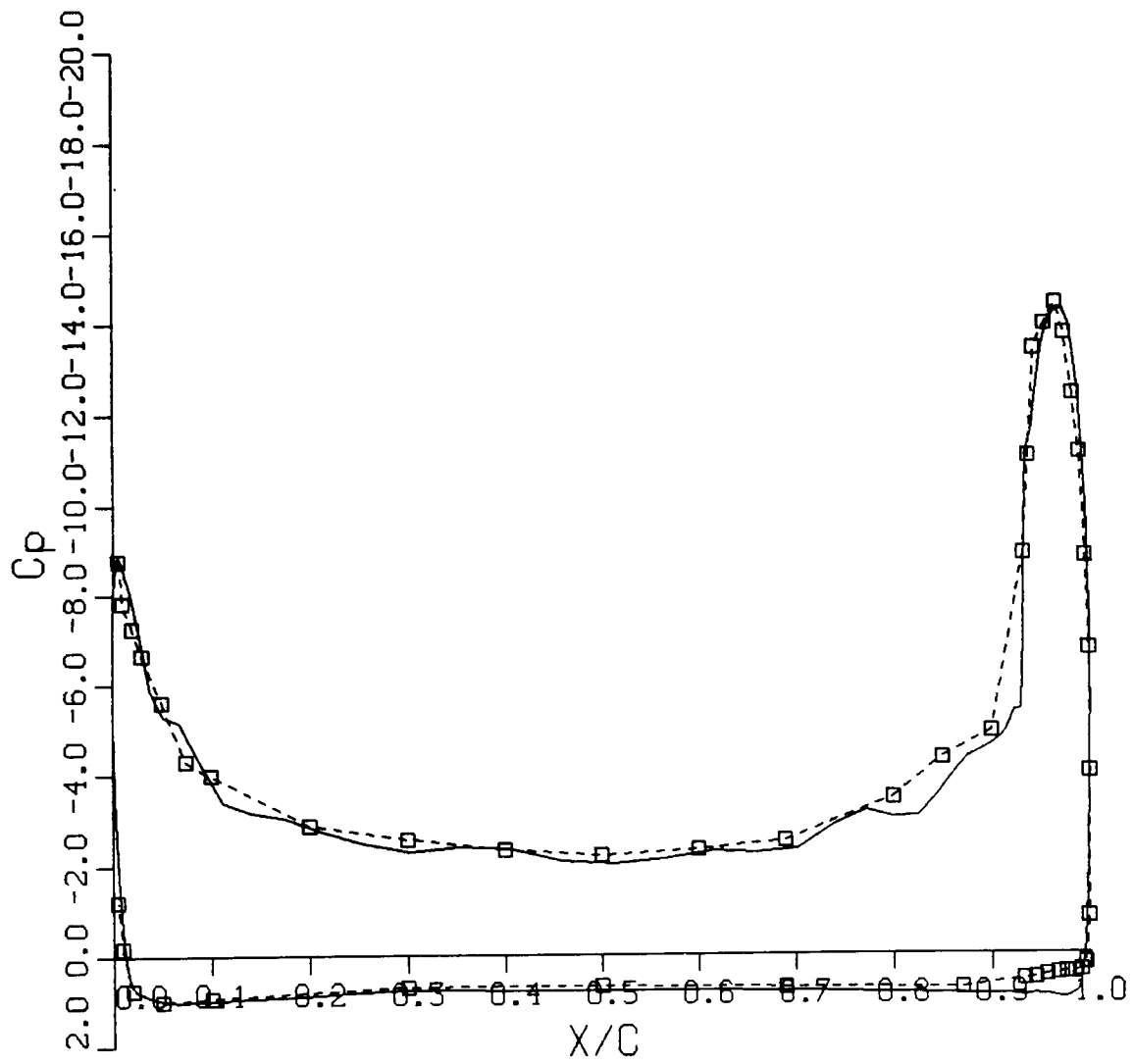


Figure 7. Computed and Experimental Pressure Coefficient Distributions